1 **Coupling of excitation energy to photochemistry in natural marine phytoplankton**
2 **communities under iron stress**

3

4 Heshani Pupulewatte[a,b], Maxim Gorbunov[b], C. Mark Moore[c], Corday R. Selden[b], Thomas J. Ryan-
5 Keogh[d], Joe Furby[c], Ruth Hawley[c], Maeve C. Lohan[c], Thomas S. Bibby[c], Paul G. Falkowski[a,b,*]

6

7 **Authors information**
8 [a]Department of Chemistry and Chemical Biology, Rutgers University, New Brunswick, NJ 08854
9 [b]Environmental Biophysics and Molecular Ecology Program, Department of Marine and Coastal
10 Sciences, Rutgers University, New Brunswick, NJ 08901
11 [c]School of Ocean and Earth Science, National Oceanography Centre, Southampton, University of
12 Southampton, Southampton SO14 3ZH, United Kingdom
13 [d]Southern Ocean Carbon-Climate Observatory, CSIR, Cape Town, South Africa

14

15 [*]Corresponding author: Paul G. Falkowski falko@marine.rutgers.edu

16

17 **Author contribution**
18 M.G., C.M.M., T.S.B. and P.G.F. designed the research; H.P., C.M.M., C.R.S., T.J.R.K., J.F., R.H.
19 collected all data onboard the DY172 cruise. M.G., P.G.F., C.M.M., T.S.B., and M.L. contributed
20 new reagents/analytical tools. H.P., M.G., C.M.M., T.S.B., and P.G.F. processed and analyzed the
21 photo physiological data. H.P., M.G., and P.G.F. wrote the paper with significant input from all
22 authors.

23

24 **Competing interest**
25 The authors declare no conflict of interest.

26

29

30 **This PDF file includes:**
31   Main Text
32   Figure 1 to 4

Abstract

Oxygenic photosynthesis requires excitation energy transfer from light-harvesting complexes (LHCs) to reaction centers (RCs) to drive photochemical redox chemistry. The effective absorption cross section of RCs dynamically responds to the light environment on time scales of seconds to days, allowing rapid acclimations to changes in spectral irradiance and photoprotection under high light, thereby optimizing light absorption for photochemistry. Although energy coupling between LHC-RCs has been studied for decades in laboratory cultures, it remains poorly understood in real-world conditions, where it is potentially influenced by nutrients. In the oceans, one of the most critical micronutrients for photosynthesis is iron (Fe). To investigate the effects of Fe stress on the energetic coupling between LHC-RCs in natural phytoplankton assemblages in the Southern Atlantic Ocean, we assessed photo-physiological responses using a pair of custom-built fluorometers measuring chlorophyll-a variable fluorescence and picosecond fluorescence lifetimes. Detailed analysis based on the functional absorption cross-section of the oxygen-evolving complex, quantum yield of photochemistry, energetic connectivity of RCs, and the average lifetime of *in vivo* chlorophyll fluorescence suggested that between 10 and 25% of LHCs remain uncoupled from RCs and do not effectively contribute to photochemical charge separation. Addition of Fe to samples under trace metal-clean on-board incubations indicates relatively rapid recoupling (< 24 h) of antennae to photochemistry, followed by biophysical stabilization of recoupled complexes. Our findings highlight the crucial role of micronutrients in controlling the excitation energy transfer from LHCs to RCs in marine phytoplankton and the overall primary productivity in the real-world oceans.

Significance statement

We examined the efficiency with which absorbed solar energy is transferred to photosynthetic electron flow in natural marine phytoplankton assemblages in the Southern Atlantic Ocean. Using a unique combination of variable fluorescence and fluorescence lifetime measurements, we measured the energetic interaction between light-harvesting complexes and reaction centers responsible for generating electrons in splitting water, and hence phytoplankton growth. Our results reveal that iron plays a critical role in restoring energy transfer through multifaceted mechanisms, including the re-coupling of existing photosynthetic complexes and also the reassembly and repair of the photosynthetic apparatus. These findings underscore the importance

64 of iron in the energetic coupling of solar energy to photochemistry and how phytoplankton adapt

65 to changes in nutrient supply prevailing in real-world oceans.

66

67 **Introduction**

68 All oxygenic photoautotrophs convert light into chemical bond energy through a suite of light-

69 dependent reactions. The initial light-dependent reaction photochemically splits water with a

70 specific, unique catalyst, Photosystem II (PSII). This process generates electrons and protons,

71 which are ultimately used to reduce carbon dioxide, and depending on the environment, nitrate

72 and sulfate (1). The first challenge photosynthetic organisms face is capturing light, which is a

73 relatively dilute energy source, even in the upper ocean. Reaction Centers (RCs), protein

74 complexes responsible for charge separation, contain relatively few light harvesting pigments;

75 hence, they can absorb only a few photons each second. Indeed, without an increase in the

76 functional absorption cross section of PSII (σ_{PSII}), oxygenic photosynthesis would be extremely

77 slow (1-3). To increase photon capture, the RCs are energetically coupled to light harvesting

78 complexes (LHCs). These pigment binding antenna complexes, which are themselves incapable

79 of photochemistry, greatly increase the cross-section of the RC, but only if they are energetically

80 coupled (2).

81 Biophysically, LHCs act as energy funnels, in which typically shorter wavelengths of light are

82 absorbed by peripheral LHCs. Excitation energy is transferred between pigments within the LHCs

83 to RCs via Förster's resonant energy-transfer (FRET) mechanism. In 1946, Förster described the

84 rate of energy transfer ($k_{Förster}$) between a donor and acceptor chromophore as dependent on the

85 donor lifetime (τ_D), the quantum yield of the donor fluorescence (φ_D), the interchromophore

86 distance (R), the relative orientation of the donor−acceptor pair (κ), and the overlap integral (J_F)

87 (4). Recent studies focus on the development of new excitonic energy levels shared between

88 strongly interacting molecules, which explain the quantum mechanical nature of excitation energy

89 transfer (5). FRET occurs along a downhill energy gradient towards the RC, where charge

90 separation is restricted by kinetics (3). Charge separation and stabilization should occur at a much

91 faster rate than the decay of an excited-state chlorophyll *a* molecule (k_d). In nutrient-replete

92 oxygenic organisms, k_d averages ca. 0.5 ns^{-1} (6). However, if FRET impedes, the excess absorbed

93 energy is dissipated either as heat or fluorescence (7, 8). Hence, the interactions between pigments

94 within the LHCs, and the energetic coupling to the RCs, critically determine how efficiently
95 absorbed solar energy is converted to electron flow.

96 Fine-tuning the energy transfer process between LHCs and RCs is essential for photosynthetic
97 organisms to adapt to environmental variability, including light and nutrients (9-11). In the ocean,
98 the paucity of nutrients, in particular, can lead to a substantial decrease in the photosynthetic
99 electron transfer efficiency (12). Nearly every macromolecular complex in the electron transport
100 chain in thylakoid membranes depends on Fe. Hence, Fe limitation significantly affects light
101 harvesting and excitation transfer to RCs across 30% to 60% of the upper global ocean (13). The
102 presence of uncoupled LHCs under Fe stress was initially studied by Riethman et al. (14) and
103 Greene et al. (15). "Uncoupled" LHCs are defined as light harvesting complexes that are unable
104 to transfer excitation energy to the RCs. Although many of these studies were conducted in
105 cyanobacteria (16), uncoupling has been observed in Fe-stressed laboratory cultures of the red
106 alga, *Rhodella violacea* (17), the green algae, *Dunaliella tertiolecta* (18) and *Chlamydomonas*
107 *reinhardtii* (19), and the diatom *Phaeodactyum. tricornutum* (15). Lin et al. (20) were the first to
108 document extraordinarily long *in situ* chlorophyll fluorescence lifetimes due to Fe stress in the
109 global ocean, which they attributed to inactive RCs and uncoupled LHCs. However, little is known
110 about how intermolecular energy transfer is affected by environmental conditions in natural
111 phytoplankton communities.

112 Here we report the effects of Fe stress on PSII functionality and FRET dynamics in natural and
113 nutrient amended marine phytoplankton communities of the South Atlantic Ocean collected on the
114 Royal Research Ship (RRS) *Discovery* (expedition DY172) from December 21, 2023, to January
115 24, 2024. A total of 22 nutrient addition experiments were performed along a transect that extended
116 south from the South African coast to the marginal ice zone of the Weddell Gyre then back to the
117 South Atlantic subtropical gyre (Fig. 1B).

118 To assess FRET efficiency, we used two different custom-built fluorometers. The first measures
119 the kinetics of variable chlorophyll fluorescence from microseconds to several milliseconds. This
120 Fluorescence Induction Relaxation (FIRe) instrument is used to quantify the quantum yield
121 photochemistry ($\varnothing_P$), and a suite of associated characteristics including variable fluorescence e.g.
122 maximal fluorescence, F_m, minimal fluorescence, F_o, quantum yield of PSII photochemistry,

123 F_v/F_m, Functional absorption cross section of PSII, σ_{PSII}, and the connectivity of energy between

124 RCs, ρ (21). The second is a picosecond lifetime fluorescence (PicoLiF) instrument, which

125 measures the exponential decay of chlorophyll fluorescence (as quantified using the lifetime τ), in

126 the picosecond to nanosecond time domain. This measurement allows for the quantification of the

127 quantum yield of fluorescence ($\o_F$) *in vivo*. Both instruments are extremely sensitive; the

128 measurements are obtained simultaneously and do not require filtration of natural phytoplankton

129 assemblages. The latter is critical; in the open ocean the average chlorophyll concentration *in situ*

130 is ~0.2 µg/l and often less (22). Filtration takes many minutes to hours, during which time the

131 relevant photosynthetic parameters can change significantly. Combining the two, independent

132 fluorescence measurements allow closure on the energy budget of absorbed solar radiation in

133 phytoplankton *in situ* based on the equations of Strasser and Butler's formalism (7, 12). The

134 research presented here reveals that a significant population of LHCs are often poorly coupled

135 energetically to photochemistry *in situ* due to Fe limitation.

136 **Results**

137 **The combination of variable chlorophyll fluorescence and picosecond lifetimes shows**
138 **signatures of uncoupling of LHCs and RCs under severe Fe stress**

139 We examined photo-physiology across the upper ocean from the high-latitude South Atlantic

140 (60°S) to the eastern South Atlantic Gyre (Fig. 1). Nutrient addition experiments were conducted

141 using various factorial combinations of inorganic Fe, Nitrogen (N), Phosphorus (P), and

142 Manganese (Mn). Subsamples for photo-physiology were taken at time points of 0, 24, and 48 h

143 after nutrient additions. Photo-physiological parameters used in this study are explained in detail

144 (See Materials and Methods and SI Appendix, Table S1). From our measurements, dFe

145 concentrations remained below 0.2 nM (SI Appendix, Table S2) and limited phytoplankton growth

146 rates south of the STF. Experiments conducted north of the STF were co-limited by Fe and N (SI

147 Appendix, Fig. S1).

148 Fe enrichment led to increases in F_v/F_m in all experiments south of the STF (Fig. 2 and SI

149 Appendix, Fig. S2). The strongest responses were seen in the APF, where measured dissolved Fe

150 concentrations were less than 0.1 nM (Fig. 2, SI Appendix, Table S1, and Fig. S3). In this region,

151   F_v/F_m increased by 90 to 120% compared to control samples, indicating severe Fe limitation. F_o

152   was reduced by 30% to 45% following Fe addition, while F_m did not change significantly,

153   reflecting decreases in F_m/Chl alongside increasing chlorophyll concentrations. Moreover, the

154   σ_{PSII}, reduced by 10 to 20%, within 48 h (SI Appendix, Fig. S3).

155

156   **10-25% LHCs remain uncoupled from RCs**

157   A linear ($R^2 = 0.85$) inverse relationship between τ and F_v/F_m was observed across all experiments

158   conducted in the study region (Fig. 3A) suggesting that as the photosynthetic energy conversion

159   efficiency decreases, more absorbed excitation energy is dissipated via fluorescence (7). Indeed,

160   F_v/F_m was exceptionally low (0.25 ± 0.06) in control treatments, while τ was relatively long (1.37

161   ± 0.18 ns). After the addition of Fe, F_v/F_m increased to 0.42 ± 0.04 and τ reduced to 0.81 ± 0.09 ns

162   (SI Appendix, Table S3). Similar to Fe alone, the supply of Fe in combination with Mn or N also

163   significantly decreased values of τ and increased values of F_v/F_m in all experiments (Fig. 3A).

164   The basic biophysical model for energy distribution in the photosynthetic unit predicts an inverse

165   relationship between the quantum yield of photochemistry (ϕ_P), and the quantum yield of

166   fluorescence (ϕ_F) (8, 20). Using this relationship, the coupling of absorbed excitation energy by

167   LHCs to RCs can be quantified (23, 24). As a result, τ is inversely proportional to the F_v/F_m (SI

168   Appendix, Fig. S4). As derived in SI Appendix, when all LHCs are coupled,

169                            $\tau = \tau_m (1 - F_v/F_m)$ (Equation 1)

170   where τ_m averages ca. 1.5 ns in phytoplankton communities of the Southern Ocean (25, 26). If

171   LHC-RCs are energetically coupled, as in nutrient-replete conditions, the results should follow

172   Strasser and Butler's formalism, i.e., Equation 1 (0% line in Fig. 3A). The presence of uncoupled

173   LHCs with extremely long lifetimes increases the fraction of uncoupled LHCs, resulting in a

174   distinct deviation from the classical inverse relationship predicted by Strasser and Butler's model

175   at low F_v/F_m values (Fig. 3A). Further modelling this relationship (SI Appendix, Fig. S4) to

176   quantify the proportion of uncoupled LHCs revealed that between 10 and 25% of the LHCs are

177   energetically uncoupled from the photochemistry of water splitting *in situ* (24). The addition of Fe

178   recouples the LHC-RC complexes within 24 h (Fig. 3B).

179

180   We hypothesized that when Fe was added, LHCs become energetically recoupled to

181   photochemistry before the biochemical repair of inactive RCs. We analyzed the temporal trends in

182 F_v/F_m and τ across three time points (0, 24, and 48 h) (Fig. 3B). The experimental results suggest

183 that the uncoupled LHCs decreased to virtually nil in the first phase, within 24 h ($\frac{\Delta\tau_{[0-24\,h]}}{\Delta(\frac{F_v}{F_m})_{[0-24\,h]}} = -$

184 5.55). Moreover, after 24 h, the experimental results are consistent with Strasser and Butler's

185 model of photosynthetic energy efficiency; approximately 54% of the absorbed excitation energy

186 is thermally dissipated (7, 8). The reduced slope during the latter phase between 24 to 48 h,

187 ($\frac{\Delta\tau_{[24-48\,h]}}{\Delta(\frac{F_v}{F_m})_{[24-48\,h]}} = -1.35$) indicates a deceleration in these changes, potentially due to the stabilization

188 of LHC-RC complexes and the biophysical recovery of inactive RCs.

189

190 **Discussion**

191 The results of our analysis reveal that a large fraction of LHCs is energetically uncoupled from

192 photochemistry *in situ* in the South Atlantic Ocean due to Fe-stress. Variable fluorescence

193 measurements have been used in previous field studies conducted in the High Nutrient Low

194 Chlorophyll (HNLC) waters to conclude that Fe stress leads to a significant reduction in

195 photosynthetic efficiency (27, 28). However, these measurements alone cannot accurately quantify

196 the presence of uncoupled antenna complexes. The current study is the first to use the combination

197 of fluorescence efficiency and lifetimes within Fe addition experiments to directly assess the

198 effects of Fe stress on energy coupling in natural marine phytoplankton assemblages *in situ*.

199 The changes we observed in F_v/F_m, F_o, F_m, σ_{PSII} and ρ suggest (1) that a significant portion of LHCs

200 are energetically uncoupled from RCs in Fe-limited waters of the study region, and (2) these

201 complexes can rapidly re-couple upon the addition of Fe. Our results clearly reveal that F_v/F_m

202 increases following Fe addition, due to a decrease in F_o. Similar observations in laboratory cultures

203 of a unicellular red alga, *Rhodella violacea*, led Desquilbet et al. to conclude that an increase in F_o

204 under Fe stress cannot be attributed solely to an increase in PSII, as this would also lead to a

205 comparable rise in F_v (17). Instead, these authors suggested that a disproportionately large increase

206 in F_o compared to F_v results in a greater contribution from the Photosystem I (PSI)-LHC complex

207 to the F_o signal. However, natural marine phytoplankton assemblages contain extremely low

208 concentrations of red algae, and fluorescence from PSI at physiological temperatures is negligible,

209 with virtually all fluorescence associated with PSII. Previous studies on cyanobacteria have

7

210 associated the observed rise in F_0 and increased τ to the accumulation of stress-induced

211 chlorophyll-binding proteins (e.g., IsiA) or from degradation of PSII RCs, leaving excess LHCs

212 unable to transfer energy (16, 29). HNLC regions if the ocean are dominated by diatom

213 populations, and Fe resupply has shown a significant increase in diatom abundance and biomass

214 in Fe fertilization experiments conducted in these regions (30). The isiA gene, primarily found in

215 cyanobacteria (31), has not been found in the diatom genome (32). Concerning diatoms, iron

216 starvation-induced proteins have been detected; however, the localization of these protein

217 structures is not fully understood (33). Moreover, although the presence of inactive RC's can be

218 responsible for longer τ, the shift from the Strasser and Butler's 0% reference line (Fig. 3A) much

219 longer τ's coupled with lower F_v/F_m cannot be explained only by the presence of inactive RCs (20).

220

221 We thus proffer an alternative explanation: We propose that the changes observed on F_0(/Chl) and

222 F_m(/Chl) upon Fe addition *in situ* represent recoupling of LHCs to PSII RCs. In theory, F_m, is the

223 fluorescence when the acceptor side of PSII RCs are reduced (i.e., "closed"). Under this condition,

224 photochemistry is nil, and absorbed photons are dissipated as heat or fluorescence. When LHCs

225 are energetically recoupled to RCIIs through the addition of Fe, F_m did not change significantly

226 and F_0(/Chl) decreased. Moreover, Fe limitation increases the fraction of inactive RCs, thus

227 increasing the physical distance between the remaining active RCs and reducing the probability of

228 exciton transfer between them, as evidenced by extremely low values of ρ (Fig. 2G). Fe enrichment

229 leads to the repair of inactive centers and the recovery in ρ (Fig. 2G, 4D).

230

231 Fe stress also significantly influences the PSII functional absorption cross section, σ_{PSII} (Fig. 2F

232 and 4C). Upon addition of Fe, a pronounced increase in σ_{PSII} was observed at 24 h in EXS2 and

233 EXS8, in the Sub Antarctic zone, suggesting an initial response to Fe supplementation (Fig. 4C,

234 SI Appendix, Fig. S5). Notably, EXS2 and EXS8 exhibited the lowest F_v/F_m (0.230 ± 0.004, 0.231

235 ± 0.009) values and the longest τ (1.269 ± 0.144 ns, 1.175 ± 0.060 ns) values, respectively,

236 indicating that these locations experienced the most severe Fe stress in the studied area. Vassilev

237 et al. reported changes to σ_{PSII} upon addition of Fe to Fe-stressed cultures of the green alga,

238 *Dunaliella tertiolecta* (18). Similar to our observations, they observed that, under extreme

239 limitation, σ_{PSII} and F_v/F_m were initially low, but increased rapidly to their respective maxima,

240 upon addition of Fe; σ_{PSII} subsequently declined while F_v/F_m remained elevated. Both σ_{PSII} and

241 F_v/F_m then reached steady-state levels after ca. 30 h at room temperature (18). Both these results

242 and the findings presented here (Fig. 4A-D) thus indicate that, under Fe limitation, LHCs are

243 coupled to the few remaining functional PSII RCs, reducing the probability of exciton energy

244 transfer from LHCs to the RCs, due to the weakened interaction with its acceptor-side chlorophyll

245 molecules of the RC; this is a so-called "puddle" model of excitation transfer (Fig. 4E) (34). This

246 may cause inefficient excitation energy transfer in the uncoupled LHCs, where energy will be lost

247 before reaching the RC, reducing the measured σ_{PSII}, and increasing τ, under Fe stress (Fig. 4B

248 and 4C). The initial increase of σ_{PSII} over the first 24 h (Fig. 4C) can be then explained by the rapid

249 reconnection of uncoupled LHCs to photochemically functional domains, causing an apparent

250 enhancement of the size of the photosynthetic unit, explained as the 'lake' model (Fig. 4C and 4E).

251 This change is then followed by the addition of newly activated or synthesized RCs, which reduces

252 the effective cross section of the antenna serving RCs. Indeed, a significant decline in σ_{PSII} (T=24

253 to T=48 h) was detected mirroring the latter phase (Fig. 4C) as previously observed in the culture

254 (18). Notably, experiments conducted in the Sub Antarctic zone (Fig. 2 and Fig. 4), appeared to be

255 the most severely Fe-stressed in these conditions; the rest exhibit a more moderate Fe stress

256 response. Experiments conducted in the South Atlantic gyre, north of the Sub Tropic Front

257 indicated N limitation (SI Appendix, Fig. S1), suggesting that N stress affects photosynthesis

258 differently. In contrast to the Fe addition response observed in Fe-stressed waters, addition of N to

259 N-stressed waters increased σ_{PSII} and F_m, due to increased chlorophyll (i.e. LHC) synthesis.

260 Combining the $\o_P$ from variable fluorescence and $\o_F$ from picosecond lifetime measurements, we

261 quantified the fraction of uncoupled LHCs, estimating that between 10% and 25% of the antenna

262 complexes are energetically uncoupled. Diel studies conducted by Park et al. (24) in the Amundsen

263 Sea polynyas (Antarctica) recorded fluorescence lifetimes in the range of 0.7–1.3 ns in the absence

264 of Fe stress with up to 25% LHCs uncoupled. Sherman et al. (35) examined diel changes in

265 photosynthetic parameters in the Equatorial Atlantic, where they showed that 25-40% of LHC-RC

266 complexes remain uncoupled and that they recouple due to upwelling. However, these efforts

267 lacked direct Fe manipulations, trace metal clean methodology, and measurements of Fe

268 concentrations, therefore, it was not possible to fully link observed photo-physiological changes

269 to Fe-limitation.

270 The combined results of the fluorescence lifetimes and observations of σ_{PSII}, included within direct

271 experimental manipulations, indicate that the region of study was subjected to Fe stress, and we

272 were able to validate that changes observed in variable fluorescence were indeed due to LHC-RC

273 uncoupling and not confounded by alternative photo-physiological processes. Prior studies (e.g.,

274 27) that estimated proportions of uncoupled LHCs have largely used models derived from only

275 variable fluorescence. While responses in variable fluorescence parameters are more commonly

276 used to deduce reasons behind photo-physiological changes, they provide only indirect evidence

277 of excitation energy transfer. In contrast, fluorescence lifetime measurements provide a direct way

278 to measure the $\o_F$ and assess the energy dissipation state of the photosynthetic machinery more

279 accurately. Therefore, this approach provides an accurate mechanistic understanding of Fe stress

280 responses in natural phytoplankton communities and represents an important methodological

281 advancement for *in situ* oceanographic studies.

282 Our results provide the first demonstration of *in situ* temporal dynamics of the interactions between

283 LHC-RC complexes and the restoration of photosynthetic function upon Fe resupply. Further, t

284 experimental data strongly suggest that re-stabilization of photosynthesis upon Fe addition is

285 multi-faceted. Firstly, the recoupling of LHC-RC complexes results in a significantly higher rate

286 of change of τ than F_v/F_m, as a response to Fe addition to Fe-stressed phytoplankton. Within the

287 first 24 h of Fe addition, data points migrate to the Strasser and Butler's 0% reference line, while

288 reducing the percentage of uncoupled LHCs, with higher changes in fluorescence lifetime than

289 F_v/F_m, (Fig. 3B) suggesting that spatial changes in distance or orientation of RC and LHCs is

290 responsible for the recoupling and reduction of fluorescence emission during this phase. Nunn et

291 al. (36) conducted quantitative proteomics in a diatom under Fe stress, indicating the loss of RCs.

292 Moreover, studies have shown that Fe limitation led to a loss of PSII subunits D1, CP43 and CP47

293 and a gain of D2 and cytb$_{559}$, in isolated thylakoid membranes (15, 18, 27, 36). Repair of these

294 components upon Fe addition, implies the recoupling and stabilization of LHC-RC complexes and,

295 stabilization of LHC-RC complexes as shown by the higher rate of change of F_v/F_m during the

296 second phase between 24-48 h, where data points follow the Strasser and Butler's relationship.

297 **Why do phytoplankton have a pool of uncoupled LHCs?**

The value to phytoplankton of producing a large pool of uncoupled antenna under Fe-stress is not well understood. Due to the large size of photosynthetic machinery and the complexity of intermolecular interactions between its sub-units, a growing number of *in vitro* and *in silico* experiments have been conducted to study intra-molecular energy transfer in isolated photosynthetic proteins, especially LHCs (37, 38). Laboratory-based studies imply that LHC-RC super complexes are highly variable; subjecting these cells to various changes can result in PSII cores with different amounts of LHCs and minor light-harvesting proteins attached. The heterogeneity of PSII RCs in nutrient replete conditions within thylakoid membranes has been visualized by using phase contrast cryo-electron tomography by Levitan et al (39). They provided proof of 2 distinct sub-populations of PSII RCs associated with and without LHCs in thylakoid membranes isolated from *Phaeodactylum tricornutum* and proposed that RCs unassociated with LHCs serve as physically isolated repair stations where photochemically damaged proteins (e.g., D1) can be removed and replaced with functional structures (39).

Uncoupled RCs may help protect the photosynthetic apparatus from photodamage. If LHC-RCs remain coupled, excess light energy can accumulate in the photosystem without being utilized effectively and may thus increase the risk of photodamage. To reduce such damage, phytoplankton may uncouple their LHCs from RCs to reduce energy capture, resulting in less energy needs to be processed downstream in the electron transport chain. Under Fe-stress, phytoplankton need to optimize the balance between energy absorption and the capability of the photosynthetic machinery to use that energy effectively. Subsequent steps in the photosynthetic electron transport chain also have high requirements for Fe. The reduced energetic connectivity between LHC-RCs can help to prevent energy imbalance by maintaining the rate of excitation at the PSII RC chlorophylls, more in line with the reduced rate of electron transfer, which is hindered by limited Fe. Sudden environmental changes such as light intensity or nutrient fluxes can occur on faster timescales than protein and pigment turnover rates. Therefore, uncoupled LHCs may also serve as a pigment reserve which can rapidly increase photosynthetic efficiency under conditions of Fe supply (16, 40).

Our results suggest that the uncoupled antenna produced under Fe limitation can significantly influence the energy balance of phytoplankton in the ocean and thereby affect the overall primary production of the South Atlantic Ocean, emphasizing the need for the incorporation of *in situ* and

328 *in vivo* fluorescence studies to accurately understand how nutrient availability affects
329 photosynthetic machinery in marine phytoplankton and the importance of understanding the
330 reasons and mechanisms behind the uncoupling phenomenon.

331 **Materials and Methods**

332 **3.1 Nutrient additions experiments**
333 The cruise track facilitated nutrient addition experiments to be conducted over a large temperature
334 gradient and range of both dissolved macronutrient and dFe concentrations (SI Appendix, Table
335 S1). Nutrient addition experiments were set up and conducted under trace metal clean conditions
336 in a class-100 clean air laboratory container as explained in detail by Wyatt et al. (41). Surface
337 seawater (2 to 3 m) for experiments was pumped directly into the clean laboratory using a Teflon
338 diaphragm pump (A-15, Almatec) connected by acid-washed PVC tubing to a towed "Fish"
339 sampler. Samples for initial (T_0) measurements (photo-physiology, chlorophyll a, and
340 macronutrients) were collected at the beginning, middle (i.e., after all experimental bottles were
341 ~50% full), and end of the filling process, with dFe (0.2 μm) samples also collected at the
342 beginning and end. Separate replicate bottles were amended with single or combination additions
343 of Fe and Mn, to final concentrations of 2 nM using $FeCl_3$ and $MnCl_2$, respectively, and prepared
344 following the detailed procedure in Wyatt et al. (41). N and P were added as 10 mM KNO_3/10 mM
345 NH_4Cl and 1mM $NaHPO_4$ to a final concentration of 1 μM. Combinations of Fe, Mn were used in
346 experiments conducted in the South Antarctic Zone, and further south, and Fe, N when in the SAG.
347 Control bottles, with no added nutrients, were collected in parallel. Following nutrient amendment,
348 the bottles were closed, then externally sealed with film (Parafilm^{TM}) and incubated in a
349 temperature-controlled container set to approximate sea surface temperature of the stations ranging
350 from 6.0 to 24.0°C (SI Appendix, Table S2). The incubation environment was maintained using
351 daylight simulation LED light banks with ~200 μmol photons m^{-2} s^{-1} flux and set to an
352 approximate local day/night cycle of 16 and 8 h, respectively.
353

354 **3.2 Dissolved Iron measurements**
355 Flow injection analysis with chemiluminescence detection (FIA-CL) was used to determine
356 nanomolar concentrations of dFe in the nutrient addition experiments (42). Briefly, each sample
357 was spiked 1 hour prior to analysis with 60 μl 0.01 M H_2O_2 and left to equilibrate, to allow any

358 present Fe(II) to be oxidized to Fe(III) (43). The sample was then buffered in-line to pH 3.5, and

359 pre-concentrated onto the cation exchange resin Toyopearl-AF-Chelate 650 M (Tosohaas).

360 Following a rinse step of 0.013 M HCl to remove the bulk seawater matrix, the Fe(III) was

361 liberated from the resin using 0.24 M HCl and entered the reaction stream with luminol, NH_4OH

362 and H_2O_2 to induce the chemiluminescent oxidation of luminol, detected by a photomultiplier tube.

363 Each sample was measured in triplicate, with a detection limit (3σ) of 0.05 ± 0.02 nM (n = 11).

364 Accuracy was established by repeat quantification of dFe in an internal reference standard

365 (ZIPLOC 1; 0.3 nM), yielding a concentration of 0.34 ± 0.02 nM (n = 7), which agrees with the

366 consensus value.

367

368 **3.3 Variable fluorescence and picosecond lifetime fluorescence**

369 Photo-physiology measurements were conducted at time points of T=24, T=32, T=48 h in short

370 experiments ('EXS') and T=48, T=96 h in large experiments ('EXL') to assess short-term and

371 long-term responses. Measurements included 3 technical replicates for each biological replicate

372 (i.e., each bottle). Variable chlorophyll fluorescence measurements were made using a

373 Fluorescence Induction Relaxation (FIRe) instrument (44). A saturating single turnover flash (STF)

374 from blue light-emitting diodes (450 ± 30 nm half bandwidth) was used to cumulatively reduce all

375 PSII RCs within ca. 80 µs. Data from the FIRe was analyzed to derive values of the minimum and

376 maximum fluorescence (F_o and F_m, respectively) and the photochemical efficiency of photosystem

377 II, ϕ_P,

378                    $\phi_P = F_v / F_m$, where $F_v = (F_m - F_o)$

379 Functional absorption cross-section of PSII (Å^2) in a dark-adapted state, σ_{PSII} (at 450 nm), was

380 calculated by fitting the fluorescence rise to a cumulative one-hit Poisson function. σ_{PSII} is the

381 product of the optical absorption cross section of PSII (i.e., the physical size of the PSII unit) and

382 the quantum yield of photochemistry in PSII. "Connectivity factor", ρ is a parameter that defines

383 the excitation energy transfer between individual photosynthetic units of PSII (dimensionless).

384

385 The PicoLiF fluorometer was used to record fluorescence kinetics in open photosynthetic RCs.

386 The kinetic signal at the F_o level (τ) was induced by laser excitation with low average optical power

387 density of 0.1 mW·cm^{-2} (21). The PicoLiF measured picosecond fluorescence decays which were

388 deconvoluted from the instrument response function and then fitted to a sum of three exponentials

with a custom TCSPFIT Matlab package (45). The quantum yield of fluorescence $\o_F$ was then calculated from,

$$\o_F = \tau_{observed}/\tau_{natural}$$

$\tau_{observed}$ is the measured lifetime and $\tau_{natural}$ is the natural lifetime of a chlorophyll a molecule (46, 47). $\tau_{natural}$ is the time that would be required for a molecule to return to the ground state from an excited state if fluorescence were the sole dissipation pathway. For Chl a, $\tau_{natural}$ is 15 ns and is constant, independent of solvent, organism or environmental condition (23). Percentage change was calculated as $\frac{(Fe\ Treatment_{48\ h} - Control_{48\ h})}{Control_{48\ h}} \times 100\%$ (See Fig. 2A and SI Appendix Fig. S3). Differences between the various response variables within the experiments were assessed using ANOVA followed by a Tukey's HSD comparison test ($P < 0.05$)

Data availability
All data is included in the manuscript and/or supporting information.

References

1.   P. G. Falkowski, R. J.A., *Aquatic Photosynthesis* (Princeton University Press, ed. 2, 2007).
2.   R. E. Blankenship, *Molecular mechanisms of photosynthesis* (Blackwell Science, ed. 1, 2002).
3.   R. Croce, H. van Amerongen, Natural strategies for photosynthetic light harvesting. *Nat Chem Biol* **10**, 492-501 (2014).
4.   T. Forster, Energiewanderung und Fluoreszenz. *Naturwissenschaften* **33**, 166–175 (1946).

423   5.   T. Mirkovic *et al.*, Light Absorption and Energy Transfer in the Antenna Complexes of
424   Photosynthetic Organisms. *Chem Rev* **117**, 249-293 (2017).
425   6.   E. Belgio, M. P. Johnson, S. Juric, A. V. Ruban, Higher plant photosystem II light-
426   harvesting antenna, not the reaction center, determines the excited-state lifetime-
427   both the maximum and the nonphotochemically quenched. *Biophys J* **102**, 2761-
428   2771 (2012).
429   7.   W. L. Butler, R. J. Strasser, Tripartite model for the photochemical apparatus of green
430   plant photosynthesis. *Proc. Natl. Acad. Sci. U.S.A.* **74**, 3382-3385 (1977).
431   8.   W. L. Butler, Energy distribution in the photochemical apparatus of photosynthesis.
432   *Ann Rev Plant Physiol* **29**, 345-378 (1978).
433   9.   S. Izawa, N. E. Good, Effect of salts and electron transport on the conformation of
434   isolated chloroplasts. II. Electron microscopy. *Plant Physiol.*, 544-552 (1966).
435   10.   A. V. Ruban, M. P. Johnson, Visualizing the dynamic structure of the plant
436   photosynthetic membrane. *Nat Plants* **1**, 15161 (2015).
437   11.   L. M. Wlodarczyk *et al.*, Functional rearrangement of the light-harvesting antenna
438   upon state transitions in a green alga. *Biophys J* **108**, 261-271 (2015).
439   12.   M. Y. Gorbunov, P. G. Falkowski, Using chlorophyll fluorescence to determine the
440   fate of photons absorbed by phytoplankton in the world's oceans. *Annu Rev Mar Sci*
441   **14**, 213-238 (2022).
442   13.   M. J. Behrenfeld, A. J. Milligan, Photophysiological expressions of iron stress in
443   phytoplankton. *Ann Rev Mar Sci* **5**, 217-246 (2013).
444   14.   H. C. Riethman, L. A. Sherman, Purification and characterization of an iron stress-
445   induced chlorophyll-protein from the cyanobacterium *Anacystis nidulans* R2.
446   *Biochim. Biophys. Acta* **935**, 141-151 (1998).
447   15.   R. M. Greene, R. J. Geider, P. G. Falkowski, Effect of iron limitation on photosynthesis
448   in a marine diatom. *Limnol. Oceanogr.* **36**, 1772-1782 (1991).
449   16.   T. J. Ryan-Keogh, A. I. Macey, A. M. Cockshutt, C. M. Moore, T. S. Bibby, The
450   cyanobacterial chlorophyll-binding-protein IsiA acts to increase the in vivo effective
451   absorption cross-section of PSII under iron limitation. *J Phycol* **48**, 145-154 (2012).
452   17.   T. E. Desquilbet, D. Jean-Claude, B. Robert, J. Houmard, J. C. Thomas, In the
453   unicellular red alga *Rhodella violacea* iron deficiency induces an accumulation of
454   uncoupled LHC. *Plant Cell Physiol.* **44** 1141–1151 (2003).
455   18.   I. R. Vassiliev *et al.*, Effects of iron limitation on photosystem II composition and
456   light utilization in *Dunaliella teutiolecta*. *Plant Physiol.* **109**, 963-972 (1995).
457   19.   J. L. Moseley *et al.*, Adaptation to Fe-deficiency requires remodeling of the
458   photosynthetic apparatus. *The EMBO Journal* **21**, 6709-6720 (2002).
459   20.   H. Lin *et al.*, The fate of photons absorbed by phytoplankton in the global ocean.
460   *Science* **351**, 264-267 (2016).
461   21.   M. Y. Gorbunov, P. G. Falkowski, Using picosecond fluorescence lifetime analysis to
462   determine photosynthesis in the world's oceans. *Photosynth Res* **159**, 253-259
463   (2024).
464   22.   M. J. Behrenfeld *et al.*, Satellite-detected fluorescence reveals global physiology of
465   ocean phytoplankton. *Biogeosciences*, 779–794 (2009).

466 23. M. A. Palacios, F. L. de Weerd, J. A. Ihalainen, R. van Grondelle, H. van Amerongen,
467   Superradiance and exciton (de)localization in light-harvesting complex II from green
468   plants. *J. Phys. Chem. B* **106**, 5782-5787 (2002).
469 24. J. Park *et al.*, Light availability rather than Fe controls the magnitude of massive
470   phytoplankton bloom in the Amundsen Sea polynyas, Antarctica. *Limnol. Oceanogr.*
471   **62**, 2260-2276 (2017).
472 25. F. I. Kuzminov, M. Y. Gorbunov, Energy dissipation pathways in Photosystem 2 of the
473   diatom, Phaeodactylum tricornutum, under high-light conditions. *Photosynth Res*
474   **127**, 219-235 (2016).
475 26. J. Sherman, M. Y. Gorbunov, O. Schofield, P. G. Falkowski, Photosynthetic energy
476   conversion efficiency in the West Antarctic Peninsula. *Limnol. Oceanogr.* **65**, 2912-
477   2925 (2020).
478 27. P. G. Falkowski, R. M. Greene, R. J. Geider, Physiological limitations on
479   phytoplankton productivity in the ocean. *Oceanography* **5**, 84-91 (1992).
480 28. R. M. Greene, Z. S. Kolber, D. G. Swift, N. W. Tindale, P. G. Falkowski, Physiological
481   limitation of phytoplankton photosynthesis in the eastern equatorial Pacific
482   determined from variability in the quantum yield of fluorescence. *Limnol. Oceanogr.*
483   **39**, 1061-1074 (2003).
484 29. R. L. Burnap, T. Troyan, L. A. Sherman, The highly abundant chlorophyll-protein
485   complex of iron-deficient Synechococcus sp. PCC7942 (CP43') is encoded by the
486   isiA gene'. *Plant Physiol.* **103**, 893-902 (1993).
487 30. H. J. W. de Baar *et al.*, Synthesis of iron fertilization experiments: From the iron age
488   in the age of enlightenment. *Journal of Geophysical Research: Oceans* **110** (2005).
489 31. U. Geiss *et al.*, Detection of the isiA gene across cyanobacterial strains: potential for
490   probing iron deficiency. *Appl Environ Microbiol* **67**, 5247-5253 (2001).
491 32. C. Bowler *et al.*, The Phaeodactylum genome reveals the evolutionary history of
492   diatom genomes. *Nature* **456**, 239-244 (2008).
493 33. E. Kazamia *et al.*, In vivo localization of iron starvation induced proteins under
494   variable iron supplementation regimes in Phaeodactylum tricornutum. *Plant Direct*
495   **6**, e472 (2022).
496 34. K. Bernhardt, H. W. Trissl, Theories for kinetics and yields of fluorescence and
497   photochemistry: how, if at all, can different models of antenna organization be
498   distinguished experimentally? *BBA* **1409** (1999).
499 35. J. Sherman *et al.*, The photophysiological response of nitrogen-limited
500   phytoplankton to episodic nitrogen supply associated with tropical instability waves
501   in the Equatorial Atlantic. *Frontiers in Marine Science* **8**, 1-14 (2022).
502 36. B. L. Nunn *et al.*, Diatom proteomics reveals unique acclimation strategies to
503   mitigate Fe limitation. *PLoS One* **8**, e75653 (2013).
504 37. E. Kim, S. Akimoto, R. Tokutsu, M. Yokono, J. Minagawa, Fluorescence lifetime
505   analyses reveal how the high light-responsive protein LHCSR3 transforms PSII light-
506   harvesting complexes into an energy-dissipative state. *J. Biol. Chem.* **292**, 18951-
507   18960 (2017).

508   38.   S. Caffarri, K. Broess, R. Croce, H. van Amerongen, Excitation energy transfer and
509   trapping in higher plant Photosystem II complexes with different antenna sizes.
510   *Biophys J* **100**, 2094-2103 (2011).
511   39.   O. Levitan *et al.*, Structural and functional analyses of photosystem II in the marine
512   diatom Phaeodactylum tricornutum. *Proc. Natl. Acad. Sci. U.S.A.* **116**, 17316-17322
513   (2019).
514   40.   M. J. Behrenfeld *et al.*, Controls on tropical Pacific Ocean productivity revealed
515   through nutrient stress diagnostics. *Nature* **442**, 1025-1028 (2006).
516   41.   N. J. Wyatt *et al.*, Phytoplankton responses to dust addition in the Fe-Mn co-limited
517   eastern Pacific sub-Antarctic differ by source region. *Proc. Natl. Acad. Sci. U.S.A.*
518   **120**, e2220111120 (2023).
519   42.   K. Kunde *et al.*, Iron distribution in the Subtropical North Atlantic: The pivotal role of
520   colloidal iron. *GBC* **33**, 1532-1547 (2019).
521   43.   M. C. Lohan, A. M. Aguilar-Islas, K. W. Bruland, Direct determination of iron in
522   acidified (pH 1.7) seawater samples by flow injection analysis with catalytic
523   spectrophotometric detection: Application and intercomparison. *Limnol.*
524   *Oceanogr.: Methods* **4**, 164-171 (2006).
525   44.   M. Y. Gorbunov, P. G. Falkowski, Using chlorophyll fluorescence kinetics to
526   determine photosynthesis in aquatic ecosystems. *Limnol. Oceanogr.* **66**, 1-13
527   (2020).
528   45.   J. Enderlein, R. Erdmann, Fast fitting of multi-exponential decay curves. *Optics*
529   *Communications* **134**, 371-378 (1997).
530   46.   J. R. Lakowicz, *Principles of fluorescence spectroscopy* (Springer, ed. 3, 2010).
531   47.   S. S. Brody, E. Rabinowitch, Excitation lifetime of photosynthetic pigments in vitro
532   and in vivo. *Science*, 555 (1957).
533   48.   M. H. Rio, S. Guinehut, G. Larnicol, New CNES-CLS09 global mean dynamic
534   topography computed from the combination of GRACE data, altimetry, and in situ
535   measurements. *J. Geophys. Res. Oceans.* **116**, 1-25 (2011).
536   49.   S. Swart, S. Speich, I. J. Ansorge, J. R. E. Lutjeharms, An altimetry-based gravest
537   empirical mode south of Africa: 1. Development and validation. *J. Geophys. Res.*
538   *Oceans.* **115**, 1-19 (2010).
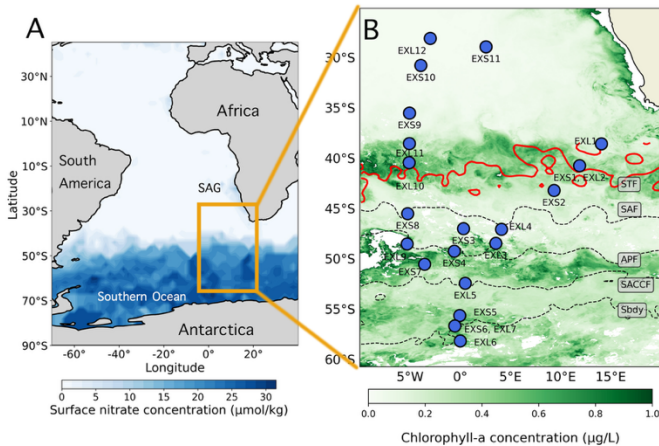539

Figure captions

Fig. 1 A. Map showing study area covering the South Atlantic Gyre (SAG) and High Nutrient Low Chlorophyll (HNLC) Southern Ocean with surface nitrate concentration in µmol/kg (World Ocean Atlas Data 2023) B. December 2023 – January 2024 Chlorophyll-a concentration in µg/L (Modis AQUA satellite retrievals at 4 km resolution). Fronts from north to south: Sub Tropical Front- STF (red), Sub Antarctic Front- SAF, Antarctic Polar Front- APF, Southern Antarctic Circumpolar Current Front- SACCF and Southern boundary- Sbdy. The positions of the fronts were determined by maps of absolute dynamic topography (ADT, m) from the (CLS-AVISO product (48) using previously defined boundary definitions (49). Markers indicate the locations where nutrient addition experiments were conducted.
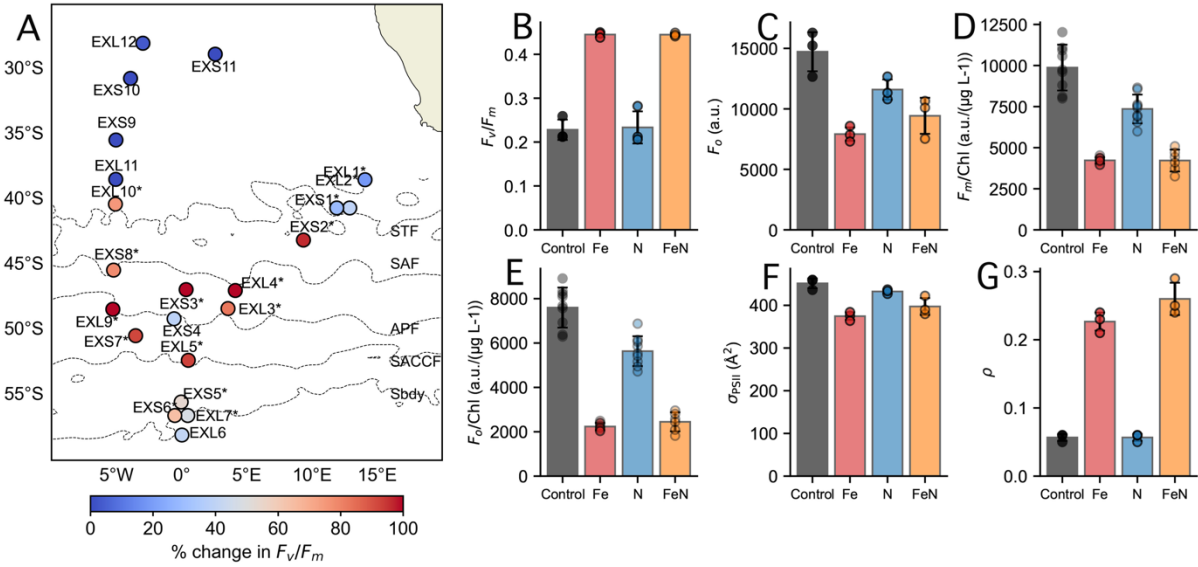
Fig. 2 A. Spatial distribution of percentage change in F_v/F_m in incubation experiments 48 h after Fe addition to final concentrations of 2 nM. Experiments where statistically significant results were obtained are indicated by * based on results of ANOVA followed by Tukey Honest Significant Difference post-hoc test. ($P \leq 0.05$). Markers used for experiments indicate the percentage size of response observed in F_v/F_m upon Fe addition according to provided color scale. The approximate latitudes of the STF, SAF, APF, SACCF, and the Sbdy are indicated by dotted lines. Example responses of photo physiological parameters, B. F_v/F_m, C. F_o D. Maximal fluorescence per chlorophyll concentration F_m/Chl, E. Minimal fluorescence per chlorophyll concentration F_o/Chl, F. σ_{PSII}, and G. ρ, 48 h after nutrient amendments of Control (black), Fe only (red), N only (blue) and Fe, N (orange) in experiment EXS7.
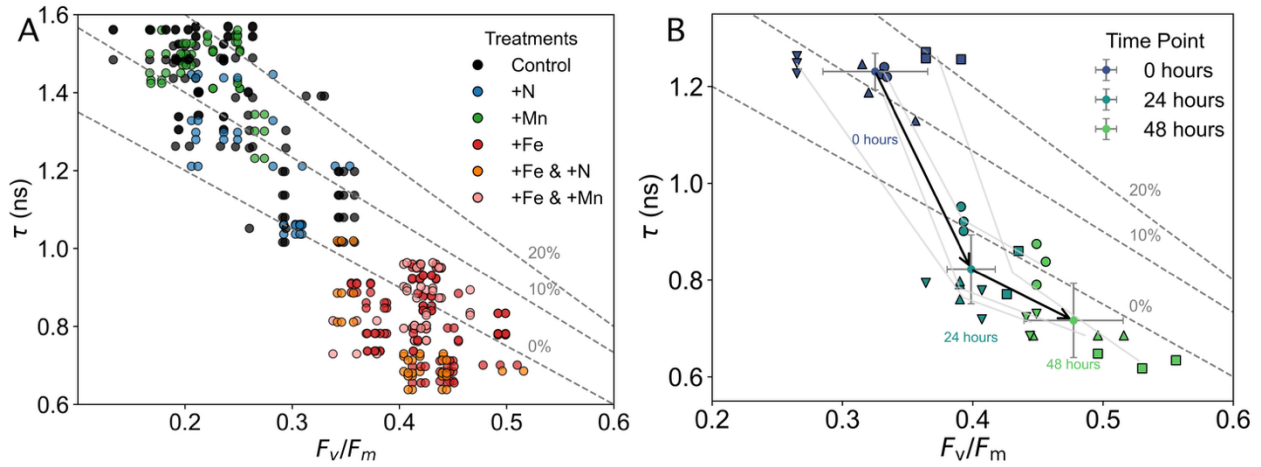
Fig. 3 A. Relationship between fluorescence lifetimes and F_v/F_m after 48 h of nutrient additions in Fe-stressed regions. The gray line with 0% mark is the theoretical dependence between the fluorescence lifetime and F_v/F_m. Gray lines (labelled as 10 to 20%) are the modeled dependence between F_v/F_m and τ, when 10–20% of the LHCs are energetically decoupled from the photosynthetic RCs (Derivation included in SI Appendix). B. Temporal trends in the changes of F_v/F_m and τ in response to Fe addition in experiments EXS3 (circle marker), EXS5 (square marker), EXS6 (triangle marker), EXS7 (inverted triangle marker).

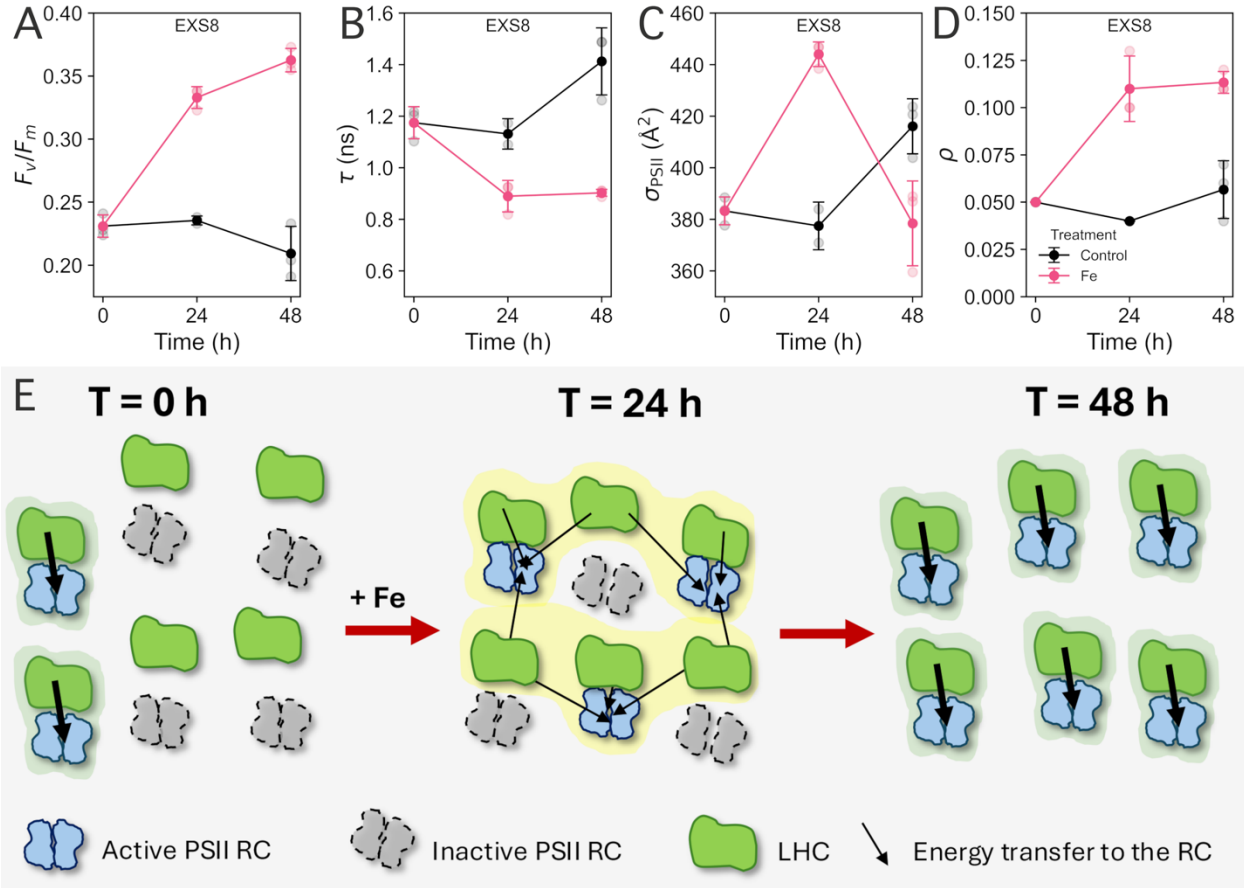Fig. 4: Example responses in A. F_v/F_m, B. τ, C. σ_{PSII}, and D. ρ, with time (T=0 h, T=24 h, and T=48 h) following the addition of Fe in experiment EXS8 (see SI Appendix, Fig. S5 for comparable plot from EXS2) E. Schematic representation of modifications in the photosynthetic machinery upon transition from Fe-stressed to nutrient-replete conditions.